Antiviral Research 161 (2019) 53–62

Contents lists available at ScienceDirect

Antiviral Research

journal homepage: www.elsevier.com/locate/antiviral

RA-839, a selective agonist of Nrf2/ARE pathway, exerts potent anti-rotaviral efficacy *in vitro*

Upayan Patra, Urbi Mukhopadhyay, Rakesh Sarkar, Arpita Mukherjee, Mamta Chawla-Sarkar*

Division of Virology, National Institute of Cholera and Enteric Diseases, P-33, C.I.T. Road Scheme- XM, Beliaghata, Kolkata 700010, India

ARTICLE INFO

Keywords:
RA-839
Rotavirus
Agonist
Nrf2/ARE (antioxidant response element) pathway
Therapeutic potential

ABSTRACT

Acute watery diarrhea due to Rotavirus (RV) infection is associated with high infantile morbidity and mortality in countries with compromised socio-economic backgrounds. Although showing promising trends in developed countries, the efficacy of currently licensed RV vaccines is sub-optimal in socio-economically poor settings with high disease burden. Currently, there are no approved anti-rotaviral drugs adjunct to classical vaccination program. Interestingly, dissecting host-rotavirus interaction has yielded novel, non-mutable host determinants which can be subjected to interventions by selective small molecules. The present study was undertaken to evaluate the anti-RV potential of RA-839, a recently discovered small molecule with potent and highly selective agonistic activity towards cellular redox stress-sensitive Nuclear factor erytheroid-derived-2-like 2 (Nrf2)/Antioxidant Response Element (ARE) pathway. *In vitro* studies revealed that RA-839 inhibits RV RNA and protein expression, viroplasm formation, yield of virion progeny and virus-induced cytopathy independent of RV strains, RV-permissive cell lines and without bystander cytotoxicity. Anti-RV potency of RA-839 was subsequently identified to be independent of stochastic Interferon (IFN) stimulation but to be dependent on RA-839's ability to stimulate Nrf2/ARE signaling. Interestingly, anti-rotaviral effects of RA-839 were also mimicked by 2-Cyano-3, 12-dioxo-oleana-1, 9(11)-dien-28-oic acid methyl ester (CDDO-Me) and Hemin, two classical pharmacological activators of Nrf2/ARE pathway. Overall, this study highlights that RA-839 is a potent antagonist of RV propagation *in vitro* and can be developed as anti-rotaviral therapeutics.

1. Introduction

Infantile deaths and morbidity due to Rotavirus (RV)-induced gastroenteritis are major impediments to socio-economic welfare in developing nations (Aliabadi et al., 2016; Clark et al., 2017; Tate et al., 2016). Introduction of vaccination programmes has shown promising trends in reducing the severity of RV disease burden (Bhandari et al., 2014; Burnett et al., 2017; Isanaka et al., 2017; Parashar et al., 2016). In endemic settings of developing countries, however, co-circulation of multiple genotypes, occurrences of mixed infections and zoonotic transmission have contributed to intergenotypic reassortments. Rotaviral diversity is further intensified by rapid accumulation of point mutations in the antigenic epitopes of viral proteins coupled to immune selection pressure imparted by the host giving rise to temporal and spatial shifts of predominant viral strains (Banerjee et al., 2018; Dóró et al., 2015; McDonald et al., 2009). In face of this unceasing viral heterogeneity, prophylactic vaccination as the sole mode of disease management might be greatly challenged over long term. Moreover, targeting highly mutable viral proteins with antivirals might only act as an impetus to host-virus evolutionary arms race leading to emergence of drug-resistant viral strains (Irwin et al., 2016; Strasfeld and Chou, 2010). Emerging evidence suggests that critical host determinants might serve as broad-range therapeutic candidates due to their indispensability for viral propagation and low mutation rates compared to viral proteins (de Chassey et al., 2012; Lee and Yen, 2012). Manipulation of pro-viral and antiviral host determinants with antagonists and agonists has, indeed, been reported to have remarkable impacts on RV propagation (Bagchi et al., 2012; Bhowmick et al., 2014; Chanda et al., 2015, 2016; Chattopadhyay et al., 2013, 2017; Crawford et al., 2012; Ding et al., 2018; Dutta et al., 2009; Eichwald et al., 2012; Holloway and Coulson, 2006; Mukherjee et al., 2018; Silva-Ayala et al., 2013; Yin et al., 2018a, 2018b). Thus, adjunct to prophylactic vaccination, developing anti-rotaviral therapeutics by targeting critical host determinants would be of prime importance to minimize selection pressure on RV strains and to reduce disease burden of rotaviral gastroenteritis.

* Corresponding author. Division of Virology, National Institute of Cholera and Enteric Diseases, P-33, C.I.T. Road, Scheme-XM, Beliaghata, Kolkata, 700010, West Bengal, India.

E-mail addresses: chawlam70@gmail.com, chawlasarkar.m@icmr.gov.in (M. Chawla-Sarkar).

https://doi.org/10.1016/j.antiviral.2018.11.009
Received 10 September 2018; Received in revised form 14 November 2018; Accepted 16 November 2018
Available online 19 November 2018
0166-3542/ © 2018 Elsevier B.V. All rights reserved.

RV, a non-enveloped virus belonging to the family *Reoviridae,* consists of a genome of 11 segmented double stranded RNAs which code for six structural (VP1-VP4, VP6 and VP7) and six non-structural (NSP1-NSP6) proteins. While infecting the enterocytes, triple layered infectious virions (called Triple Layered Particles or TLPs) shed their outermost layer to form double-layered particles (DLPs) which become transcriptionally active within host cytosol. Assisted by VP2 and VP3, VP1 initiates transcription within DLPs to form capped, non-polyadenylated, plus-strand RNAs which serve as both messengers for viral protein translation and templates for replication of the viral genome. Viral genome replication within DLPs and early viral morphogenesis occur in highly dynamic, electron-dense aggregates within host cytoplasm, called viroplasms, the formation of which also requires NSP5 along with its hyperphosphorylated isoforms and NSP2 (Desselberger, 2014; Estes and Greenberg, 2013; Silvestri et al., 2004). Upon virus infection, like other un-physiological cellular stimuli, eukaryotic cells evoke adaptive, homeostatic stress response genes some of which are also innate immune regulators of infection. Disturbing the exquisite balance in the spatio-temporal regulation of host stress responses is often how viruses subvert host innate immunity to ensure obligatory intracellular propagation (López et al., 2016).

Adaptive cellular responses against oxidative and electrophilic stresses are largely orchestrated by Nuclear factor erytheroid-derived-2-like 2 (Nrf2), a member of the 'cap-n-collar' class of basic leucine zipper transcription factor. Under unstressed conditions, trans-activation potencies of Nrf2 are restricted by keeping Nrf2 sequestered in cytosol by Kelch-like erythroid cell-derived protein with CNC homology [ECH]-associated protein 1 (Keap1), a cysteine-rich adaptor of Cullin3-Ring Box1 (Cul3-Rbx1) E3 ubiquitin ligase complex. Stoichiometrically, two Kelch domains of Keap1 dimers interact with the high affinity 'ETGE' and low affinity 'DLG' motifs of one Nrf2 molecule at Neh2 domain, one of Nrf2's six functional Nrf2-ECH homology domains (Neh1-6), orienting the Nrf2 molecule for ubiquitination by Cul3-Rbx1 complex. Prompt proteasomal degradation of ubiquitinated Nrf2 renders the Keap1 dimers free for sequestering additional nascent Nrf2 molecules thereby repeating the cycle and accounting for low basal expression of Nrf2. When challenged by oxidative and electrophilic stresses, subsets of the cysteine residues in Keap1 are covalently modified leading to a conformational change in the protein and release of Nrf2 from the low affinity binding sites. At this 'locked' conformation, Keap1 can bind only to high affinity binding sites of Nrf2; thus, transfer of ubiquitin to and subsequent proteasomal degradation of Nrf2 are hampered. In absence of free Keap1 repressors, nascent Nrf2 molecules translocate to nucleus, heterodimerize with small musculoaponeurotic fibrosarcoma (sMaf) proteins and bind to Antioxidant Response Element (ARE), the canonical cis-acting enhancer sequence (TCAG/CXXXGC) in the promoter region of Nrf2-regulated genes, to produce anti-oxidant and cytoprotective effectors. (Baird et al., 2014; Bryan et al., 2013; Harder et al., 2015; Niture et al., 2014; Suzuki et al., 2016; Tong et al., 2006, 2007).

RA839 [(3S)-1-[4-[(2, 3, 5, 6-tetramethylphenyl) sulfonylamino]-1-naphthyl] pyrrolidine-3-carboxylic acid] was initially identified as a non-covalently and very specifically interacting small molecule of Keap1 (K_d ~6 μm). Moreover, unlike non-selective, covalent Keap1 modifiers such as sulforaphane, oltipraz, CDDO-Me, RA-839 selectivity induced Nrf2/ARE pathway without bystander cytotoxicity (Winkel et al., 2015). Effects of RA-839 on RV replication were observed while studying the dynamics between RV infection and host redox-stress response. Interestingly, RA-839 was found to efficiently reduce RV RNA and protein expression, viroplasm formation and infectious progeny yield *in vitro* at sub-cytotoxic doses. Detailed mechanistic investigations revealed anti-RV potential of RA-839 to be independent of stochastic Interferon induction and relying partially on RA-839's ability to stimulate Nrf2/ARE signaling. Together, the study highlights an excellent therapeutic potential of RA-839, a non-covalent, highly selective inducer of Nrf2/ARE pathway, against rotaviral propagation *in vitro*.

2. Materials and Methods

2.1. Cell culture and virus infection

Monkey kidney cell line MA104 (ATCC number: CRL-2378™) was cultured in Minimal Essential Medium (MEM) and human colorectal adenocarcinoma cell line HT29 (ATCC number: HTB-38™), human embryonic kidney cell line HEK293 (ATCC number: CRL-1573™), human alveolar epithelial cell line A549 (ATCC® CCL-185™) were cultured in Dulbecco's Modified Eagle's Medium (DMEM) as described previously (Dutta et al., 2011). Cell culture adapted RV strains SA11 (simian strain; G3P[2]), A5-13 (bovine strain; G8P[1]), Wa (human strain; G1P[8]) and EW (murine strain) were used in this study. Unless otherwise mentioned, cells were infected at a multiplicity of infection (moi) 1 in all experiments as described previously (Dutta et al., 2011). The time of virus addition was considered as 0 hour post infection (0 hpi) for all experiments (Chattopadhyay et al., 2013).

2.2. Viral infectivity assay

For calculating viral infectivity, plaque assay was performed according to protocols described previously (Bagchi et al., 2010; Dutta et al., 2009). Viral Plaque Forming Units (PFU) were calculated as PFU/ml (of original stock) = 1/dilution factor x number of plaques x 1/(ml of inoculum/plate) (Smith et al., 1979). Relative viral load of drug-treated infected cells was represented as '% of infectivity' considering infectivity of vehicle-treated infected control as 100% in each replicate of quadruplicate experiments.

2.3. Reagents and antibodies

RA-839 (5707) was purchased from Tocris and was dissolved in Dimethyl sulfoxide (DMSO) to form a stock solution of 40 mM. Dilution of the stock solution was carried out in MEM or DMEM. CDDO-Methyl Ester (SMB00376), Hemin (H9039), Cordycepin (C3394), phosphatase inhibitor cocktail 2 (P5726), protease inhibitor cocktail (P2714) and MTT (M5655) were purchased from Merck (Sigma-Aldrich). RA-839, CDDO-Me, Hemin, Cordycepin were added 1 hour post virus addition (during addition of final media). Polyclonal and Monoclonal antibodies used for this study are listed in Supplementary Table 1 and Supplementary Table 2 respectively and were used according to the manufacturer's recommended dilutions. Antisera against RV-SA11 structural and nonstructural proteins were raised either against peptide (for NSP4, NSP1) or by purification of full-length protein expressed in bacterial expression system (for VP1, VP2, NSP2, NSP3, NSP5) in rabbits according to standard protocols at the Department of Virology and Parasitology, Fujita Health University School of Medicine, Aichi, Japan.

2.4. Sub-cellular fractionation of nucleus and cytosol

Nuclear and cytosolic fractions were separated by NE-PER™ Nuclear and Cytoplasmic Extraction Reagents (78833; Thermo Scientific™) following the manufacturer's instructions.

2.5. Transfection of siRNA

Transfection of Keap1-specific (Qiagen) and scrambled siRNAs were carried out in MA104 cells with siPORT-NeoFX (Ambion) according to the manufacturer's instructions.

2.6. Western blot

Cells were washed with ice-cold PBS and lysed in RIPA buffer (Bhowmick et al., 2015). Protein concentration was measured by Bradford reagent (Sigma Aldrich) or Pierce™ BCA Protein Assay Kit (Thermo Scientific™). Whole cell lysates, cytosolic and nuclear fractions

were mixed with protein sample buffer (Bhowmick et al., 2015) and boiled for 10 minutes. Samples were further run on SDS-PAGE followed by immunoblotting with specific antibodies as described previously (Bagchi et al., 2010). Primary antibodies were detected with HRP conjugated secondary antibody (Thermo Scientific™) and chemiluminescent substrate (Millipore & Bio-Rad) within ChemiDoc Imaging System (Bio-Rad). The immunoblots shown are representatives of at least three independent experiments. Relative fold changes (with respect to the first lane) were represented below the panel of each protein after normalizing against GAPDH or Histone H3 (for proteins isolated from nuclear fraction) using Image Lab software (version 5.2.1), Biorad.

2.7. Immunofluorescence

MA104 cells, grown in four-welled chambered slides (BD Pharmingen), were infected with RV-SA11 in presence and absence of RA-839 and processed as described previously (Mukherjee et al., 2018). RV-NSP5 antiserum and DyLight488-labeled goat anti-rabbit (Thermo Scientific™) antibody were used as primary and secondary antibodies respectively. Cells were finally stained with 4′, 6′-diamidino-2-phenylindole (DAPI) (mounting medium) and covered with a cover slip. Imaging was done in Zeiss Axioplan microscope (63X oil immersion). Number of viroplasm positive cells were calculated as the mean of 'x' from five different fields of 2 biological replicates with each field having a minimum of 40 DAPI positive cells; 'x' for each field is counted as (Number of cells with punctate viroplasms/Total number of DAPI positive cells)X100.

2.8. Knockdown of Nrf2 expression by Nrf2 shRNA

Short hairpin sequences targeting Nrf2 (Forward primer- 5′-CCGG AAGCACAGCAGAATTCAATGACTCGAGTCATTGAATTCTGCTGTGCTT TTTTTG-3'; Reverse Primer- 5′-AATTCAAAAAAAGCACAGCAGAATTC AATGACTCGAGTCATTGAATTCTGCTGTGCTT-3′) were generated with the help of a siRNA Selection Program hosted by Whitehead Institute for Biomedical Research and inserted into pLKO.1 - TRC cloning vector (Addgene plasmid #10878) (Moffat et al., 2006). Transfection of Nrf2 shRNA was carried out using Lipofectamine 2000 (Invitrogen) according to manufacturers' instructions. Nrf2 knockdown efficiency was assessed by western blot from cells expressing Nrf2 shRNA using anti-Nrf2 antibody.

2.9. PCR and quantitative real time (qRT) PCR

Total cellular RNA was extracted by TRIzol reagent (Invitrogen) according to the manufacturer's instructions. cDNA was prepared from 500 ng of RNA using Superscript II reverse transcriptase (Invitrogen) with random hexamer primers by incubating at 42 °C for 1 hour. cDNA was amplified by conventional PCR method using primers listed in Supplementary Table 3. The PCR amplicons were separated in 1.5% agarose gel and visualized using Gel Documentation (Biorad). Real time PCR reactions (Bhowmick et al., 2015) were performed in triplicate using SYBR Green (Applied Biosystems) in Step one plus (Applied Biosystems) with primers listed in Supplementary Table 4. The relative gene expressions were normalized to *gapdh* using the formula $2^{-\Delta\Delta CT}$ ($\Delta\Delta CT = \Delta CT_{\text{Sample}} - \Delta CT_{\text{Untreated control}}$; CT is the threshold cycle) and represented as 'fold change decrease of RV RNA with respect to vehicle-treated control'.

2.10. Cell viability assay

To determine cytotoxicity of chemicals in MA104 cells, cell viability assays were conducted in 96-well plates at 80%–90% cell confluency. Cells were treated with chemicals (RA-839, CDDO-Me, Hemin) at indicated concentrations upto 24 or 48 hours followed by MTT assay. Briefly, 10 µL of MTT solution (5 mg/mL in PBS) was added and incubated at 37 °C for 4 h. The formazan complex was dissolved in 200 µL MTT solvent (4 mM HCl, 0.1% Nonidet P-40 in isopropanol) and the optical density (OD) of the solutions was measured at 570 nm. Percentage of cell viability was measured by the formula (OD_{Sample}-OD_{Blank}) X 100/($OD_{Control}$-OD_{Blank}).

2.11. Luciferase reporter assay

MA104 cells were transfected with Cignal antioxidant response luciferase reporter from Qiagen (336841) according to the manufacturer's recommendations. Cells were further treated with indicated concentration of RA-839 24 hours post transfection. Firefly luciferase activity was analyzed 12 hours post treatment by Dual-Luciferase® Reporter Assay System (Promega, E1910). Briefly, cells were lysed in 1X passive lysis buffer and cell lysates were mixed with luciferase assay reagent. Firefly luciferase activity was measured and finally normalized with the *Renilla* luciferase control. A positive control (with constitutive luciferase expression) was kept to check transfection efficiency.

2.12. IC50 and CC50 determination

50% inhibitory concentration (IC50) and 50% cytotoxic concentration (CC50) of RA-839 were calculated using GraphPad Prism (Version 5) software using non-linear regression model [Y = Bottom + (Top-Bottom)/(1 + 10^{(LogIC50-X)*HillSlope)}].

2.13. Statistical analyses

Mean ± standard deviation (S.D.) of at least three independent biological replicates ($n \geq 3$) was considered for analyses. For Western blot analyses, RNA quantification, luciferase reporter assay, cell viability assay, viroplasm positivity assay and plaque assay, $p < 0.05$ (Mann-Whitney *U* test and Student's *t*-test) was considered to be statistically significant. For drug interaction studies, Chou-Talalay Combination Index (CI) was evaluated by CompuSyn software using dose-dependent 'fractional inhibition' data (Chou and Talalay, 1984; Zhang et al., 2016). CI values of < 0.95, 0.95–1.05 and > 1.05 were considered as synergistic, additive and antagonistic effects respectively.

3. Results

3.1. RA-839 treatment significantly reduced RV RNA and protein expressions, viroplasm formation and infectious progeny yield in vitro

A dose response study of RA-839 (Fig. 1A) (5, 10, 20 and 40 µM) on levels of RV protein VP6 was carried out in RV-SA11 infected (12 hpi) MA104 cells as a pilot experiment. Compared to DMSO-treated infected control, treatment with 20 and 40 µM of RA-839 resulted in significant reduction of VP6 protein levels, the concentration of 40 µM being more effective and decreasing VP6 levels to near-abolishment (Fig. 1B). The possibility of bystander host cytotoxicity being the reason for stunted viral protein levels was ruled out as both 20 µM (cell viability 95.7 ± 2%) and 40 µM (cell viability 90 ± 2%) concentrations of RA-839 were found to be tolerated well by MA104 cells upto 48 hours (Supplementary Fig. 1A). A concentration of 20 µM of RA-839 was therefore chosen to conduct further experiments. RA-839 treatment in RV-SA11 infected MA104 cells caused robust and persistent reductions in the levels of structural RV proteins (VP1, VP2, VP6) both at relatively early (12 and 24 hpi) as well as late (36 and 48 hpi) time points of infection (Fig. 1C). RV non-structural protein levels (NSP1, NSP2, NSP3, NSP4, NSP5) were also found to be attenuated at 12 and 24 hours post RV-SA11 infection (Supplementary Fig. 1B). Notably, none of the polyclonal sera against RV structural and non-structural proteins tested were found to be cross-reactive to host proteins and therefore detected in uninfected control cells. RV RNA levels were further investigated in presence and absence of RA-839 in MA104 cells infected with RV-SA11.

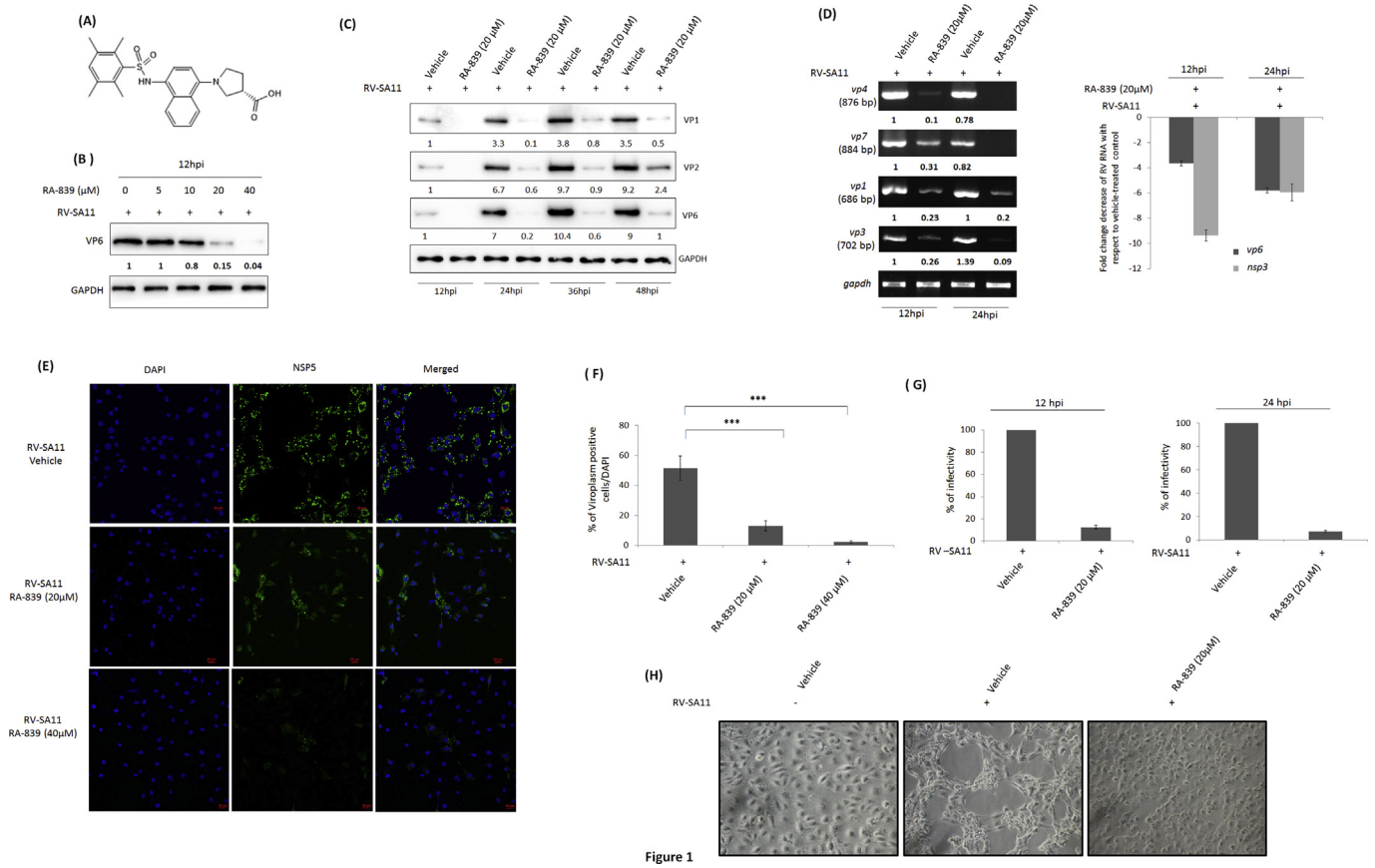

Figure 1

Fig. 1. RA-839 treatment has significant antagonistic effects on RV replication and propagation *in vitro*. **(A)** Chemical structure of RA-839 is shown. **(B)** Expression of VP6 was assessed by Western blot in RV-SA11 infected MA104 cells (12 hpi) treated with either DMSO (vehicle control) or graded concentrations of RA-839 (5, 10, 20, 40 μM). GAPDH was used as an internal loading control. Relative fold change was represented as described in Materials and Methods section (2.6.). **(C)** MA104 cells were infected with RV-SA11 (moi 0.1) in presence or absence of 20 μM RA-839. Cellular lysates prepared at 12, 24, 36 and 48 hpi were subjected to Western blot for checking expressions of RV structural (VP1, VP2, VP6) proteins. GAPDH served the purpose of internal loading control. Relative fold change was represented as described in Materials and Methods section (2.6.). **(D)** Total RNA was extracted from RV-SA11 infected MA104 cells either vehicle-treated or treated with 20 μM RA-839 (at 12 and 24 hpi); relative expressions of RV RNAs were evaluated by conventional PCR (*vp4*, *vp7*, *vp1*, *vp3*) and quantitative real time PCR (*vp6*, *nsp3*) using *gapdh* expression as normalizing control. Relative fold changes (with respect to the first lane) were represented below the panel of each gene after normalizing against *gapdh* using Image Lab software (version 5.2.1), Biorad. Fold change of viral gene expression obtained by qRT-PCR was normalized and represented as described in Materials and Methods section (2.9.). **(E)** MA104 cells were infected with RV-SA11 in presence or absence of RA-839 (20 μM and 40 μM), fixed at 12 hpi with paraformaldehyde, blocked and subsequently stained with anti-NSP5 antiserum (as a marker for viroplasms) overnight. Secondary staining and mounting were performed with Dylight488 labeled anti-rabbit antibody and DAPI respectively. Cells were finally visualized by confocal microscopy (63X oil immersion; Tiling mode); Scale bar 20 μm. **(F)** Viroplasm positivity was quantified as described in the Materials and Methods section (2.7) (Mann-Whitney test, n = 10, $***p < 0.001$). **(G)** End point viral titers (12 and 24 hpi) were measured by plaque assay from RV-SA11 infected MA104 cells treated with vehicle or 20 μM RA-839; relative infectivity of RA-839-treated samples compared to vehicle-treated counterpart was represented by '% of infectivity' as described in the Materials and Methods section (2.2.). **(H)** Morphological appearance of RA-839-treated or vehicle-treated MA104 cells infected with RV-SA11 for 24 hours was observed under light microscope (Axiovert 40 CFL; Carl Zeiss; 40X) to visualize RV-induced cytopathy.

Consistent with the marked attenuation of RV proteins in RA-839 treated cells, RV-RNA levels were also significantly low in response to RA-839 at 12 and 24 hpi in both conventional (*vp1*, *vp3*, *vp4*, *vp7*) and quantitative real time PCR-based studies (*vp6*, *nsp3*) (Fig. 1D). These results suggest that RA-839 may hamper overall RV replication in MA104 cells. The status of viroplasms was therefore investigated by confocal microscopy in presence and absence of RA-839 in MA104 cells infected with RV-SA11 using RV-NSP5 as viroplasm marker. In response to RA-839, formation of punctate viroplasms was compromised (Fig. 1E), as evident by the acute decline in the percentage of viroplasm positive cells at 12 hpi from 51.6 ± 8.19% in DMSO-treated RV-SA11 infected MA104 cells to 13.2 ± 3.43% and 2.35 ± 0.67% in presence of 20 and 40 μM RA-839 respectively (Fig. 1F). Yield of infectious viral progeny was also severely affected in response to RA-839. In comparison to DMSO-treated infected control, conventional plaque assay revealed 0.82 ± 0.13 log (87.54 ± 1.75%) and 1.34 ± 0.12 log (92.5 ± 0.68%) decline in viral titer at 12 and 24 hpi respectively in presence of RA-839 (Fig. 1G). Moreover, percentage of inhibition in viral yield as a result of RA-839 treatment followed a dose dependent pattern at 12, 24 as well as 48 hours post RV-SA11 infection (Supplementary Fig. 1C). Interestingly, cytopathic effects in the form of loss of cell adhesion characteristics of RV-SA11 infection were found to be substantially reduced in RA-839 treated infected cells, further asserting a robust cyto-protective and anti-rotaviral property of RA-839 (Fig. 1H). Next, the impact of RA-839 on propagation of human RV strain Wa, bovine RV strain A5-13 and murine RV strain EW was evaluated in MA104 cells. RA-839 resulted in 1.75 ± 0.1 log (94.26 ± 0.35%), 0.85 ± 0.03 log (88.23 ± 0.41%) and 0.77 ± 0.12 log (86.74 ± 2.32%) reductions of viral particle during RV-Wa (Supplementary Fig. 1D), RV-A5-13 (Supplementary Fig. 1E) and RV-EW (Supplementary Fig. 1F) infection respectively at 24 hpi. Anti-rotaviral potency of RA-839 was also observed in HT29 [1.18 ± 0.22 log (91.36 ± 1.41%) reduction of viral titer] (Supplementary Fig. 1G) and HEK293 cell line [0.88 ± 0.15 log

Table 1
IC50 values of RA-839 against different RV strains and CC50 value of RA-839 in MA104 cell line.

RV Strain	IC50 (μM)	CC50 (μM)
SA11	10.303 ± 0.397	
Wa	6.187 ± 0.204	110.035 ± 18.465
A5-13	11.97 ± 1.01	

Table 2
IC50 values of RA-839 against RV-SA11 and CC50 values of RA-839 in two different RV permissive cell lines.

Cell Line	IC50 (μM)	CC50 (μM)
HT29	11.815 ± 1.195	111.8
HEK293	9.686 ± 0.684	84.89 ± 12.38

(88.35 ± 1.9%) reduction of viral titer] (Supplementary Fig. 1H) 24 hours post RA-SA11 infection. IC50 (based on viral titer measurement at 24hpi) and CC50 values of RA839 against different RV strains and RV permissive cell lines are listed in Table 1 and Table 2. Collectively, the data suggests potent antagonistic effects of RA-839 on RV infection *in vitro*.

3.2. RA-839 is a potent agonist of Nrf2-driven transcription units

RA-839 has previously been reported to be a potent and highly specific inducer of Nrf2-dependent gene transcription (Winkel et al., 2015). Concurrently, in this study too, RA-839 treatment in MA104 cells (12 and 24 hours) resulted in increased levels of Nrf2 protein in whole cell lysates as well as in purified nuclear fractions (Fig. 2A). To further assess whether RA-839-induced nuclear accumulation of Nrf2 does coincide with stimulated gene transcription from Nrf2-driven transcription units, a luciferase reporter assay was performed in presence and absence of 20 μM RA-839. As reported previously (Winkel et al., 2015), a significant up-regulation of Nrf2-driven luciferase expression was observed in cells treated with RA-839 compared to cells treated with vehicle control DMSO (Supplementary Fig. 2A). Consistently, protein levels of HO-1 and NQO1, which are regulated transcriptionally by Nrf2, were also found to be significantly elevated in presence of RA-839 (Fig. 2A). Similar effects of RA-839 on Nrf2/ARE pathway were also found in HT29 (Supplementary Fig. 2B) and HEK293 cell lines (data not shown). Interestingly, knocking down expression of Nrf2 by Nrf2 shRNA abrogated RA-839-mediated induction of Nrf2 (Fig. 2B) leading to restoration of HO-1 and NQO1 protein to basal levels (Fig. 2B). These results indicate that induction of HO-1 and NQO1 in response to RA-839 is highly Nrf2-dependent. The potency of RA-839 in up-regulating Nrf2-regulated gene transcription is dependent on its interaction with Nrf2-interacting Kelch domain of Keap1 (Winkel et al., 2015). Thus, it can be hypothesized that RA-839-mediated induction of Nrf2/ARE pathway should not be observed in cells silenced for Keap1 expression. Consistent to our hypothesis, neither Nrf2 nor HO-1 and NQO1 protein levels were found to be elevated in response to RA-839 in cells transfected with Keap1 siRNA (Fig. 2C). Basal level expressions of Nrf2, HO-1 and NQO1, however, were observed to be higher in absence of Keap1 and much alike to RA-839 treated cells (Fig. 2C). The necessity to modulate Nrf2-repressor activity of Keap1 by RA-839 for Nrf2/ARE activation was further ascertained in A549 cells. This Non-Small Cell Lung Carcinoma (NSCLC) cell line harbors an inherent mutation in the Keap1 protein rendering Keap1 incapable of interaction with Nrf2 (Singh et al., 2006). Indeed, RA-839 treatment failed to elevate protein levels of Nrf2, HO-1 and NQO1 in A549 cell line (Fig. 2D). Overall, the results suggest that RA-839 treatment leads to significant induction of Nrf2 along with Nrf2-driven gene transcription *in vitro*.

3.3. Anti-rotaviral potency of RA-839 is partially dependent on induction of Nrf2

Next, we investigated whether there is any possible correlation between RA-839's ability to exert anti-RV effects and to selectively trigger Nrf2-dependent gene transcription *in vitro*. Diminishing the pool of nascent Nrf2 by RNA interference has been shown to abrogate RA-839-mediated activation of Nrf2/ARE pathway (Fig. 2B). Anti-RV potency of RA-839 was therefore evaluated in MA104 cells in presence and absence of Nrf2 shRNA. Expressions of structural (VP1, VP6) and non-structural (NSP1, NSP3, NSP5) RV proteins, which were reduced in cells treated with RA-839 only, were partially rescued in RA-839 treated cells silenced for Nrf2 expression both at 12 and 24 hpi (Fig. 3A). Significant reductions of infectious viral progenies in presence of RA-839 [0.87 ± 0.1 log (88.38 ± 1.32%) and 1.25 ± 0.11 log (91.97 ± 0.67%) at 12 and 24 hpi respectively] were also recovered partly [0.18 log (42.96 ± 1.14%) and 0.15 ± 0.01 log (35.03 ± 5.13%) at 12 and 24 hpi respectively] in cells pre-transfected with Nrf2 shRNA in addition to RA-839 treatment (Fig. 3B). These results suggest that the anti-RV efficacy of RA-839 is partially dependent on Nrf2 induction. Owing to the insensitivity of A549 cell line to RA-839-mediated activation of Nrf2/ARE pathway (Fig. 2D), *in vitro* anti-RV impacts of RA-839 were further investigated in A549 cell line. No significant changes in the expression levels of structural (VP1, VP6) and non-structural (NSP1, NSP5) RV proteins were observed in response to RA-839 in A549 cell line at 12 and 24 hpi (Fig. 3C). Consistently, RA-839 also failed to significantly reduce end point viral titers at 12 and 24 hpi in A549 cell line (Fig. 3D), asserting the importance of Nrf2/ARE pathway in mediating anti-RV effects of RA-839. Moreover, treatment of RV-SA11 infected MA104 cells with CDDO-Me (1 μM) and Hemin (20 μM), two classical pharmacological activators of Nrf2, also resulted in 1.4 ± 0.13 log (92.81 ± 0.65%) and 0.62 ± 0.06 log (83.83 ± 1.52%) decline in viral titers respectively (Fig. 3E) at 24 hpi without loss of cell viability (87 ± 2% for CDDO-Me and 98.33 ± 5.13% for Hemin) (Supplementary Figs. 3A and B).

3.4. Anti-RV impact of RA-839 is independent of stochastic interferon induction

The possibility of non-specific IFN response (Nrf2-independent) was further investigated to contribute to RA-839-mediated anti-RV effects by assessing the activation status of Janus Kinase (JAK)1-Signal transducer and activator of transcription (STAT)1 pathway (a signature of IFN signaling induction) in response to RA-839. Cordycepin was kept as a positive control because of its previously reported role on boosting IFN signaling through activation of Retinoic Acid-Inducible Gene 1 (RIG-I)/Mitochondrial Antiviral-Signaling protein (MAVS)/phospho-Interferon regulatory factor 3 (p-IRF3) axis (Chanda et al., 2015). Interestingly, unlike Cordycepin-treated cells which showed phosphorylation of STAT1, JAK1 as well as induced levels of IRF3, p-IRF3 (Ser396) and RIG-I, RA-839 (20 μM) treatment failed to stimulate IFN signaling (Fig. 4A). Next, anti-RV potency of co-treatment of Cordycepin with RA-839 was evaluated in RV-SA11 infected MA104 cells. Cordycepin co-treatment with 20 μM of RA-839 was found to exert additive effects (CI = 1.03 at 16 μM of Cordycepin; CI = 0.99 at 32 μM of Cordycepin; CI = 1.03 at 64 μM of Cordycepin) as revealed by the end point viral titer measurement at 12hpi (Fig. 4B).

4. Discussion

Designing antiviral therapeutics targeted against deterministic host factors of viral infection and without stochastic bystander adversities has paved a new era of research. Manipulation of host regulators with therapeutic anti-RV potential has been reported at various stages of host-RV interaction, such as viral entry (Li et al., 2017; Silva-Ayala et al., 2013), cellular signaling influencing RV replication (Bhowmick

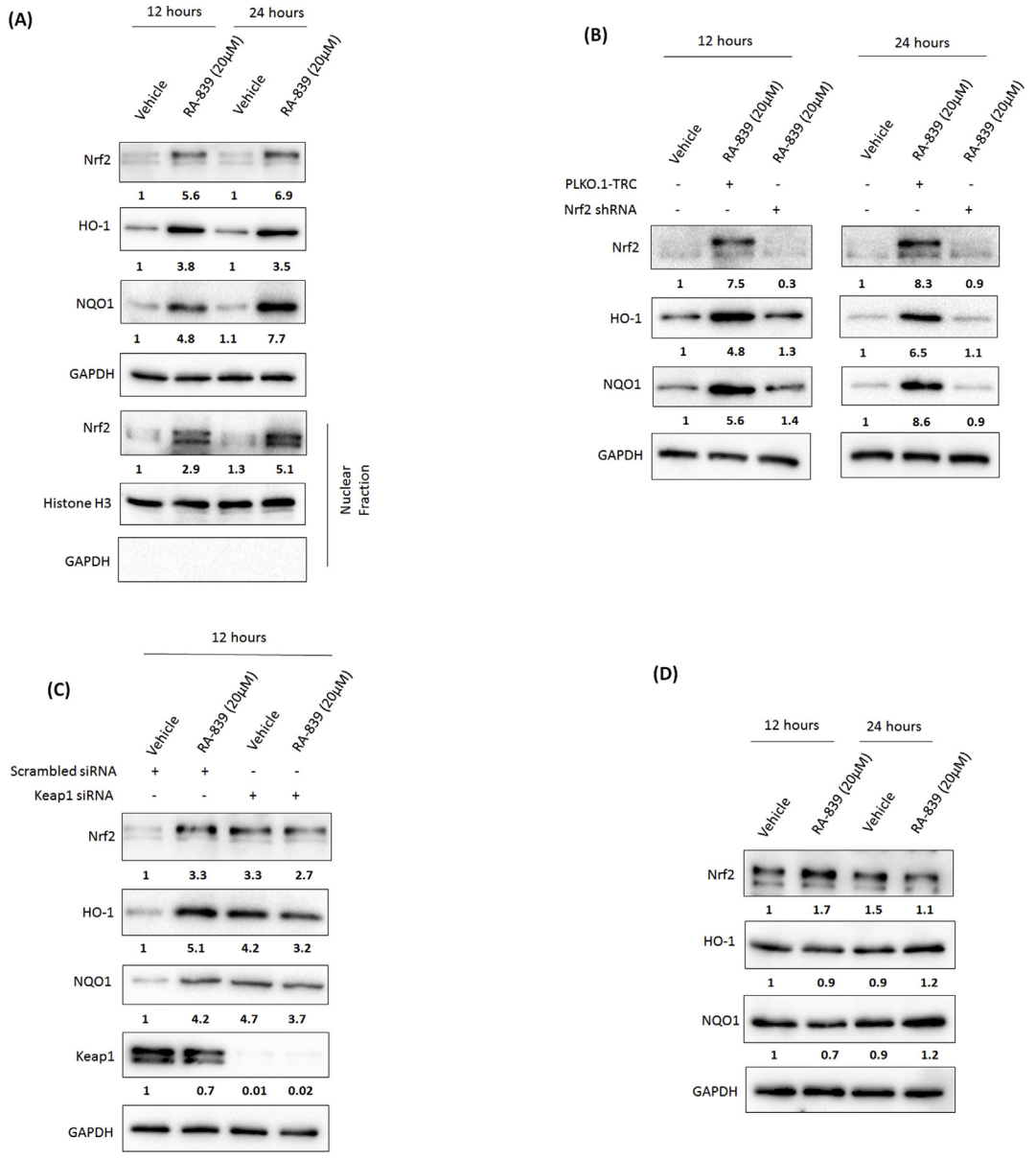

Figure 2

Fig. 2. RA-839 exerts significant agonistic activity towards activation of Nrf2/ARE pathway. **(A)** Whole cell lysates along with purified nuclear fractions prepared from DMSO-treated or 20 μM RA-839-treated MA104 cells were harvested (12 and 24 hours post treatment) and further subjected to Western Blot for assessing expressions of Nrf2 (whole cellular fraction and nuclear fraction), HO-1 and NQO1 (whole cellular fraction). GAPDH and Histone H3 were used as internal loading controls for whole cellular fraction and nuclear fraction respectively. GAPDH was also used to check sub-cellular purity of nuclear fraction. **(B)** MA104 cells, transfected with mock vector (PLKO.1-TRC) or Nrf2 shRNA (cloned into PLKO.1-TRC), were further treated with DMSO or 20 μM RA-839 36 hours post transfection. Expressions of Nrf2, HO-1 and NQO1 in whole cellular extracts were checked by Western Blot 12 and 24 hours post RA-839 treatment. Re-Probing with GAPDH served the purpose of internal loading control. **(C)** Scrambled siRNA or Keap1-specific siRNA transfected MA104 cells were treated with DMSO or 20 μM RA-839 36 hours post transfection. Whole cellular extracts (prepared after 12 hours of DMSO/RA-839 treatment) were checked for expressions of Nrf2, HO-1, NQO1 and Keap1 by Western Blot. Probing for GAPDH served the purpose of loading uniformity. **(D)** Whole cell lysates isolated from DMSO/RA-839 (20 μM)-treated A549 cells were checked for expressions of Nrf2, HO-1 and NQO-1 by Western blot. Loading equality was assured by re-probing the membrane with GAPDH. Relative fold change for each panel in each subfigure was represented as described in Materials and Methods section (2.6.).

et al., 2014; Chattopadhyay et al., 2013; Crawford et al., 2012; Yin et al., 2018b) and viroplasm dynamics (Eichwald et al., 2012), host cellular apoptosis (Bagchi et al., 2010; Chanda et al., 2016; Chattopadhyay et al., 2017; Dutta et al., 2009; Mukherjee et al., 2018), boosting of antiviral IFN signaling (Chanda et al., 2015; Dagenais et al., 1981; Ding et al., 2018; Lecce et al., 1990; Shen et al., 2013). The current study depicts the potential of RA-839 (Fig. 1A), an agonist of cellular redox-stress responsive Nrf2/ARE pathway, in remarkably restricting RV propagation *in vitro*. RA-839 treatment at a sub-cytotoxic dose (Supplementary Fig. 1A, Table 1, Table 2) resulted in marked decrease of viral titers independent of RV strains (Fig. 1G, Supplementary Figs. 1D, E, F), RV-permissive cell lines (Supplementary Figs. 1G and H) and infection time points (Fig. 1C, Supplementary Fig. 1C). Consistently, viroplasm formation was compromised in presence of RA-839 (Fig. 1E and F) leading to diminished expression of RV RNAs (Fig. 1D) and proteins (Fig. 1B and C, Supplementary Fig. 1B). These results indicate that RA-839 exerts a potent cyto-protective (Fig. 1H) anti-RV activity *in vitro*.

Characterization and biological functions of RA-839 as a selective agonist of redox stress-responsive Nrf2/ARE pathway were reported

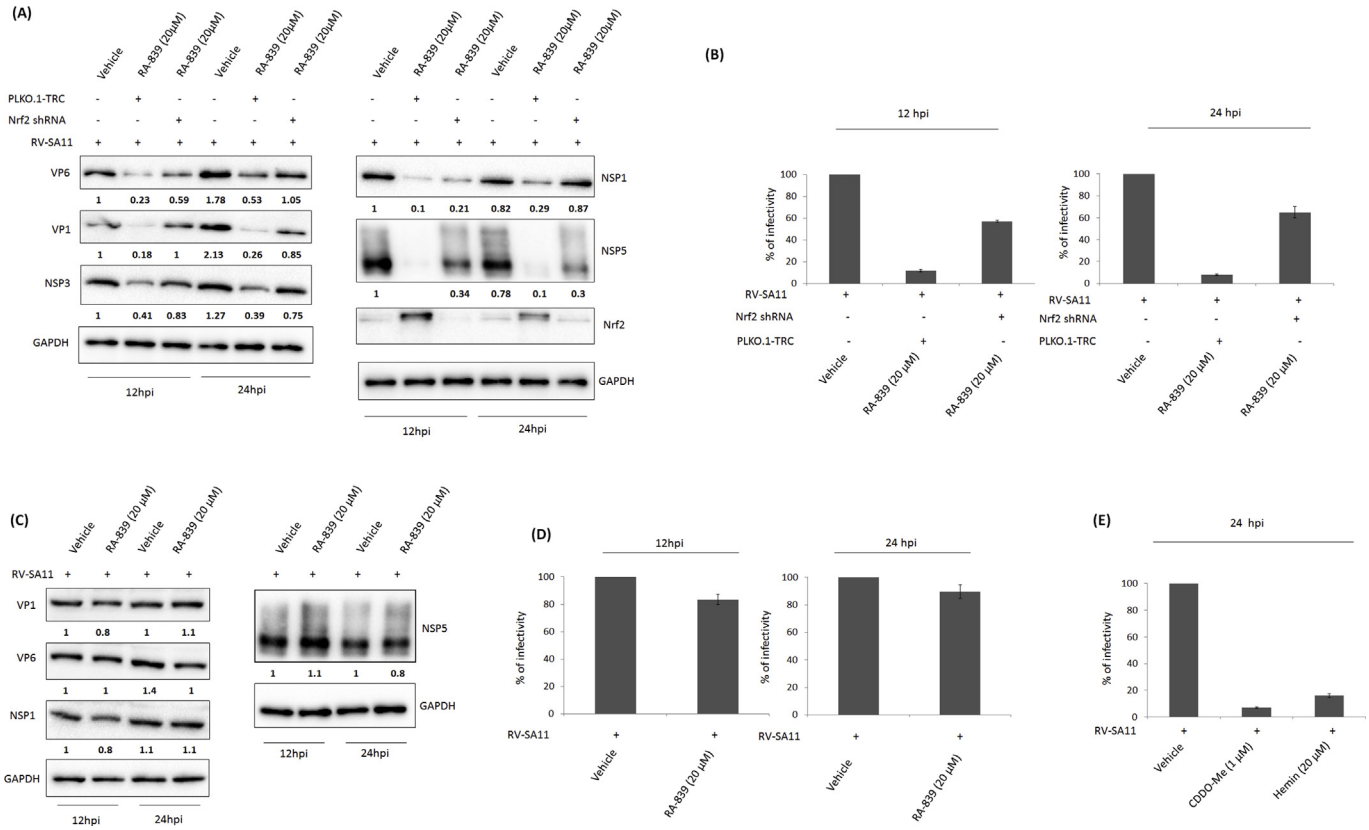

Fig. 3. RA-839 shows anti-RV effects *in vitro* by inducing Nrf2/ARE pathway. **(A)** MA104 cells were transfected with mock vector (PLKO.1-TRC) or Nrf2 shRNA and were further infected with RV-SA11 36 hours post transfection in presence of either DMSO or 20 μM RA-839. Expressions of RV structural (VP1, VP6) and non-structural (NSP1, NSP3, NSP5) proteins at 12 and 24 hpi were checked by Western blot; probing for GAPDH served the purpose of loading equality. Relative fold change was represented as described in Materials and Methods section (2.6.). **(B)** Mock vector-transfected or Nrf2 shRNA-transfected MA104 cells were subsequently infected with RV-SA11 in presence or absence of 20 μM RA-839. End point viral titers (12 and 24 hpi) were measured by plaque assay and finally represented as '% of infectivity' [described in the Materials and Methods section (2.2.)]. **(C)** Cellular lysates from RV-SA11 infected (12 and 24 hpi) A549 cells, treated with either DMSO or RA-839 (20 μM), were subjected to Western blot for assessing expressions of RV proteins (VP1, VP6, NSP1, NSP5); equal protein loading was assured by GAPDH. Relative fold change was represented as described in Materials and Methods section (2.6.). **(D)** RV-SA11 titers from infected A549 cells (12 and 24 hpi) treated with RA-839 (20 μM) were measured by plaque assay and expressed as '% of infectivity' compared to DMSO-treated infected control. **(E)** RV-SA11 titers (determined by plaque assay) at 24 hpi of vehicle-treated or CDDO-Me (1 μM) and Hemin (20 μM)-treated infected MA104 cells were represented as '% of infectivity' as described in the Materials and Methods section (2.2.).

very recently. RA-839 was found to interact with the Nrf2-interacting Kelch domain of Keap1 with a stoichiometry of 1:1 and K_d of around 6 μm. X-ray crystallography as well as thermodynamic profiling revealed the carboxylic group of RA-839 to be involved in critical ionic interactions with Arg^{415} and Arg^{483} of Keap1. Functional significance of RA-839 as a potent inducer of Nrf2-driven gene transcription was revealed by RNA quantification and luciferase reporter assay (Winkel et al., 2015). In our studies too, RA-839 treatment was found to induce stability and nuclear translocation of Nrf2 protein (Fig. 2A, Supplementary Fig. 2B) leading to upregulation of Nrf2-driven transcription units (Supplementary Fig. 2A) and protein level induction of two candidate Nrf2-responsive genes HO-1 and NQO1 (Fig. 2A, Supplementary Fig. 2B). RA-839 was speculated to dock at the Nrf2-interacting Kelch domain of Keap1 thereby rendering Keap1 dimers unavailable to nascent Nrf2 molecules. Indeed, knocking down Nrf2 by RNA interference blocked RA-839-mediated elevation of Nrf2, HO-1 and NQO1 protein levels (Fig. 2B). Interestingly, anti-RV potential of RA-839 was also significantly affected in absence of Nrf2 (Fig. 3A and B). Target specificity of RA-839 was ascertained when RA-839 failed to stimulate Nrf2, HO-1 and NQO1 protein levels in absence of either Keap1 (Fig. 2C) in Keap1 siRNA expressing cells or Keap1-Nrf2 interaction (Fig. 2D) in Keap1-mutated A549 cell line. Notably, A549 cell line was also found to be insensitive to RA-839-mediated anti-RV effects (Fig. 3C and D). These results, supported further by the anti-RV potencies of two other Nrf2 activators CDDO-Me and Hemin (Fig. 3E), indicate anti-RV efficacy of RA-839 to be partially dependent on Nrf2/ARE pathway.

Unlike most of the conventional Nrf2 activators such as sulforaphane, oltipraz, CDDO-Me, which covalently modify Keap1 cysteine residues and beckon serious safety issues associated with stochastic off-target adverse effects (Chen et al., 2014; de Zeeuw et al., 2013; Liby and Sporn, 2012; Park et al., 2011; Scannevin et al., 2012; To et al., 2010; Tran et al., 2009; Wang et al., 2014; Weerachayaphorn et al., 2014; Zoja et al., 2014) leading to their failures in pre-clinical and clinical trials, RA-839 was identified to be highly selective in stimulating Nrf2/ARE pathway at sub-cytotoxic concentration both *in vitro* and *in vivo*. Global gene expression analyses upon RA-839 treatment in Nrf2 knock out BMDM cell line revealed significant regulation of only two genes (*Zfp192* and *Pank1*) which were not regulated in wild type counterpart. Moreover, RA-839 was also shown to be unreactive in binding assays to a panel of 93 unrelated cellular proteins (Winkel et al., 2015), some of which are known regulators of RV infection [PI3K, GSK3β (Bagchi et al., 2010, 2013), mTOR (Yin et al., 2018a), AMPKα (Crawford et al., 2012), cSrc (Chattopadhyay et al., 2017), Cdk1 (Mukherjee et al., 2018), MAPK1 (Holloway and Coulson, 2006; Jafri et al., 2007), CaMKI (Bhowmick et al., 2014)]. We further nullified non-specific IFN signaling to contribute to anti-RV impacts of RA-839 (Fig. 4A). When co-administered with IFN booster Cordycepin, however, 20 μM of RA-839

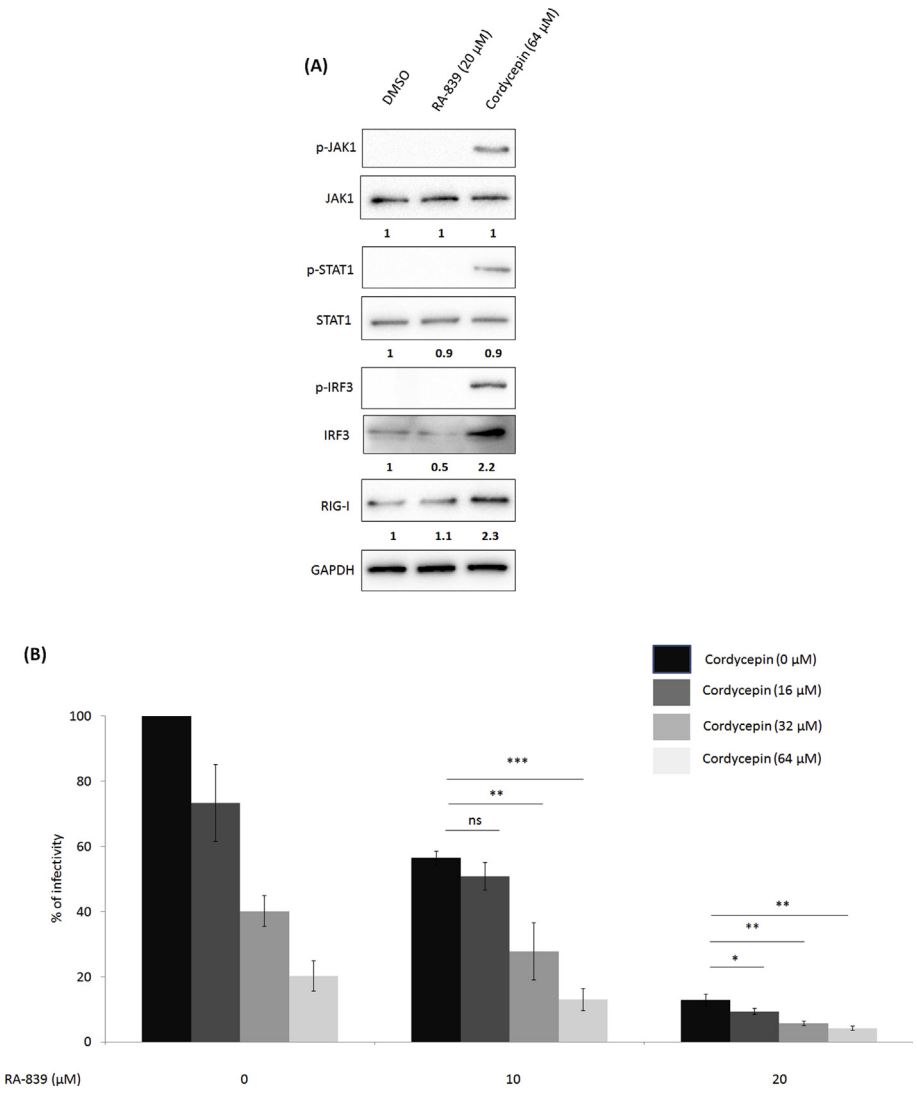

Fig. 4. (A) MA104 cells were kept treated with RA-839 (20 μM) or cordycepin (64 μM) for 12 hours before checking the expressions of p-JAK1, JAK1, p-STAT1, STAT1, p-IRF3, IRF3, RIG-I by Western Blot using GAPDH as internal loading control. Relative fold change was represented as described in the Materials and Methods section (2.6.). **(B)** Titers of RV-SA11 (at 12 hpi) from infected MA104 cells treated with indicated combinations of Cordycepin (0, 16, 32, 64 μM) and RA-839 (0, 10, 20 μM) were shown as '% of infectivity' as described in the Materials and Methods section (2.2.) (Student's t-test, n = 3, $*p \leq 0.05$, $**p \leq 0.01$, $***p \leq 0.001$, ns = non-significant).

showed additive anti-RV effects (Fig. 4B) without added cytotoxic severity.

Overall, the present study highlights the potency of RA-839, a selective agonist of Nrf2/ARE pathway, as an anti-RV therapeutic candidate *in vitro*. Owing to its metabolic instability, RA-839 possesses the added advantage of avoidance of chronic Nrf2 activation in mice (Winkel et al., 2015), further increasing its therapeutic potential. In future, it will be interesting to address the dynamics between RV infection and host redox-stress response which will further elucidate the significance of Nrf2/ARE pathway on RV infection.

Declaration of interests

None.

Acknowledgements

This study was supported jointly by extramural grants from West Bengal Higher Education, Science & Technology and Biotechnology and Department of Biotechnology (DBT)– Women Bioscientist Grant, India. UP was supported by Senior Research Fellowship from Indian Council of Medical Research (ICMR); UM, RS and AM were supported by Senior Research Fellowships from University Grants Commission (UGC). We acknowledge Division of Gastrointestinal Sciences at Christian Medical College (CMC), Vellore for providing viral strains. Asim Biswas is acknowledged for his technical assistance in confocal microscopy. Department of Virology and Parasitology, Fujita Health University School of Medicine, Aichi, Japan, is duly acknowledged for providing antisera against RV proteins.

Appendix A. Supplementary data

Supplementary data to this article can be found online at https://doi.org/10.1016/j.antiviral.2018.11.009.

References

Aliabadi, N., Tate, J.E., Parashar, U.D., 2016. Potential safety issues and other factors that may affect the introduction and uptake of rotavirus vaccines. Clin. Microbiol. Infect. Off. Publ. Eur. Soc. Clin. Microbiol. Infect. Dis. 22 (Suppl. 5), S128–S135. https://doi.org/10.1016/j.cmi.2016.03.007.

Bagchi, P., Dutta, D., Chattopadhyay, S., Mukherjee, A., Halder, U.C., Sarkar, S., Kobayashi, N., Komoto, S., Taniguchi, K., Chawla-Sarkar, M., 2010. Rotavirus non-structural protein 1 suppresses virus-induced cellular apoptosis to facilitate viral growth by activating the cell survival pathways during early stages of infection. J. Virol. 84, 6834–6845. https://doi.org/10.1128/JVI.00225-10.

Bagchi, P., Nandi, S., Nayak, M.K., Chawla-Sarkar, M., 2013. Molecular mechanism behind rotavirus NSP1-mediated PI3 kinase activation: interaction between NSP1 and the p85 subunit of PI3 kinase. J. Virol. 87, 2358–2362. https://doi.org/10.1128/JVI.02479-12.

Bagchi, P., Nandi, S., Chattopadhyay, S., Bhowmick, R., Halder, U.C., Nayak, M.K., Kobayashi, N., Chawla-Sarkar, M., 2012. Identification of common human host genes involved in pathogenesis of different rotavirus strains: an attempt to recognize probable antiviral targets. Virus Res. 169, 144–153. https://doi.org/10.1016/j.

virusres.2012.07.021.
Baird, L., Swift, S., Llères, D., Dinkova-Kostova, A.T., 2014. Monitoring Keap1–Nrf2 interactions in single live cells. Biotechnol. Adv. 32, 1133–1144. https://doi.org/10.1016/j.biotechadv.2014.03.004.
Banerjee, A., Lo, M., Indwar, P., Deb, A.K., Das, S., Manna, B., Dutta, S., Bhadra, U.K., Bhattacharya, M., Okamoto, K., Chawla-Sarkar, M., 2018. Upsurge and spread of G3 rotaviruses in Eastern India (2014-2016): full genome analyses reveals heterogeneity within Wa-like genomic constellation. Infect. Genet. Evol. J. Mol. Epidemiol. Evolut. Genet. Infect. Dis. 63, 158–174. https://doi.org/10.1016/j.meegid.2018.05.026.
Bhandari, N., Rongsen-Chandola, T., Bavdekar, A., John, J., Antony, K., Taneja, S., Goyal, N., Kawade, A., Kang, G., Rathore, S.S., Juvekar, S., Muliyil, J., Arya, A., Shaikh, H., Abraham, V., Vrati, S., Proschan, M., Kohberger, R., Thiry, G., Glass, R., Greenberg, H.B., Curlin, G., Mohan, K., Harshavardhan, G.V.J.A., Prasad, S., Rao, T.S., Boslego, J., Bhan, M.K., India Rotavirus Vaccine Group, for the I.R.V., 2014. Efficacy of a monovalent human-bovine (116E) rotavirus vaccine in Indian infants: a randomised, double-blind, placebo-controlled trial. Lancet (London, England) 383, 2136–2143. https://doi.org/10.1016/S0140-6736(13)62630-6.
Bhowmick, R., Banik, G., Chanda, S., Chattopadhyay, S., Chawla-Sarkar, M., 2014. Rotavirus infection induces G1 to S phase transition in MA104 cells via Ca + 2/Calmodulin pathway. Virology 454 (455), 270–279. https://doi.org/10.1016/j.virol.2014.03.001.
Bhowmick, R., Mukherjee, A., Patra, U., Chawla-Sarkar, M., 2015. Rotavirus disrupts cytoplasmic P bodies during infection. Virus Res. 210, 344–354. https://doi.org/10.1016/j.virusres.2015.09.001.
Bryan, H.K., Olayanju, A., Goldring, C.E., Park, B.K., 2013. The Nrf2 cell defence pathway: Keap1-dependent and -independent mechanisms of regulation. Biochem. Pharmacol. 85, 705–717. https://doi.org/10.1016/j.bcp.2012.11.016.
Burnett, E., Jonesteller, C.L., Tate, J.E., Yen, C., Parashar, U.D., 2017. Global impact of rotavirus vaccination on childhood hospitalizations and mortality from diarrhea. J. Infect. Dis. 215, 1666–1672. https://doi.org/10.1093/infdis/jix186.
Chanda, S.D., Banerjee, A., Satabdi, N., Chakrabarti, S., Sarkar, M.C., 2015. Cordycepin an adenosine analogue executes anti rotaviral effect by stimulating induction of type I interferon. J. Virol. Antivir. Res. 04, 1–12. https://doi.org/10.4172/2324-8955.1000138.
Chanda, S., Nandi, S., Chawla-Sarkar, M., 2016. Rotavirus-induced miR-142-5p elicits proviral milieu by targeting non-canonical transforming growth factor beta signalling and apoptosis in cells. Cell. Microbiol. 18, 733–747. https://doi.org/10.1111/cmi.12544.
Chattopadhyay, S., Basak, T., Nayak, M.K., Bhardwaj, G., Mukherjee, A., Bhowmick, R., Sengupta, S., Chakrabarti, O., Chatterjee, N.S., Chawla-Sarkar, M., 2013. Identification of cellular calcium binding protein calmodulin as a regulator of rotavirus A infection during comparative proteomic study. PloS One 8, e56655. https://doi.org/10.1371/journal.pone.0056655.
Chattopadhyay, S., Mukherjee, A., Patra, U., Bhowmick, R., Basak, T., Sengupta, S., Chawla-Sarkar, M., 2017. Tyrosine phosphorylation modulates mitochondrial chaperonin Hsp60 and delays rotavirus NSP4-mediated apoptotic signaling in host cells. Cell. Microbiol. 19, e12670. https://doi.org/10.1111/cmi.12670.
Chen, H., Assmann, J.C., Krenz, A., Rahman, M., Grimm, M., Karsten, C.M., Köhl, J., Offermanns, S., Wettschureck, N., Schwaninger, M., 2014. Hydroxycarboxylic acid receptor 2 mediates dimethyl fumarate's protective effect in EAE. J. Clin. Investig. 124, 2188–2192. https://doi.org/10.1172/JCI72151.
Chou, T.C., Talalay, P., 1984. Quantitative analysis of dose-effect relationships: the combined effects of multiple drugs or enzyme inhibitors. Adv. Enzym. Regul. https://doi.org/10.1016/0065-2571(84)90007-4.
Clark, A., Black, R., Tate, J., Roose, A., Kotloff, K., Lam, D., Blackwelder, W., Parashar, U., Lanata, C., Kang, G., Troeger, C., Platts-Mills, J., Mokdad, A., Global Rotavirus Surveillance Network, C., Sanderson, C., Lamberti, L., Levine, M., Santosham, M., Steele, D., 2017. Estimating global, regional and national rotavirus deaths in children aged. PloS One 12, e0183392. https://doi.org/10.1371/journal.pone.0183392.
Crawford, S.E., Hyser, J.M., Utama, B., Estes, M.K., 2012. Autophagy hijacked through viroporin-activated calcium/calmodulin-dependent kinase kinase- signaling is required for rotavirus replication. Proc. Natl. Acad. Sci. U. S. A. 109, E3405–E3413. https://doi.org/10.1073/pnas.1216539109.
Dagenais, L., Pastoret, P.P., Van den Broecke, C., Werenne, J., 1981. Susceptibility of bovine rotavirus to interferon. Brief report. Arch. Virol. 70, 377–379.
de Chassey, B., Meyniel-Schicklin, L., Aublin-Gex, A., André, P., Lotteau, V., 2012. New horizons for antiviral drug discovery from virus-host protein interaction networks. Curr. Opin. Virol. 2, 606–613. https://doi.org/10.1016/j.coviro.2012.09.001.
de Zeeuw, D., Akizawa, T., Audhya, P., Bakris, G.L., Chin, M., Christ-Schmidt, H., Goldsberry, A., Houser, M., Krauth, M., Lambers Heerspink, H.J., McMurray, J.J., Meyer, C.J., Parving, H.-H., Remuzzi, G., Toto, R.D., Vaziri, N.D., Wanner, C., Wittes, J., Wrolstad, D., Chertow, G.M., BEACON Trial Investigators, 2013. Bardoxolone methyl in type 2 diabetes and stage 4 chronic kidney disease. N. Engl. J. Med. 369, 2492–2503. https://doi.org/10.1056/NEJMoa1306033.
Desselberger, U., 2014. Rotaviruses. Virus Res. 190, 75–96. https://doi.org/10.1016/J.VIRUSRES.2014.06.016.
Ding, S., Diep, J., Feng, N., Ren, L., Li, B., Ooi, Y.S., Wang, X., Brulois, K.F., Yasukawa, L.L., Li, X., Kuo, C.J., Solomon, D.A., Carette, J.E., Greenberg, H.B., 2018. STAG2 deficiency induces interferon responses via cGAS-STING pathway and restricts virus infection. Nat. Commun. 9, 1485. https://doi.org/10.1038/s41467-018-03782-z.
Dóró, R., Farkas, S.L., Martella, V., Bányai, K., 2015. Zoonotic transmission of rotavirus: surveillance and control. Expert Rev. Anti-infect. Ther. 13, 1337–1350. https://doi.org/10.1586/14787210.2015.1089171.
Dutta, D., Bagchi, P., Chatterjee, A., Nayak, M.K., Mukherjee, A., Chattopadhyay, S., Nagashima, S., Kobayashi, N., Komoto, S., Taniguchi, K., Chawla-Sarkar, M., 2009. The molecular chaperone heat shock protein-90 positively regulates rotavirus infection. Virology 391, 325–333. https://doi.org/10.1016/j.virol.2009.06.044.
Dutta, D., Chattopadhyay, S., Bagchi, P., Halder, U.C., Nandi, S., Mukherjee, A., Kobayashi, N., Taniguchi, K., Chawla-Sarkar, M., 2011. Active participation of cellular chaperone Hsp90 in regulating the function of rotavirus nonstructural protein 3 (NSP3). J. Biol. Chem. 286, 20065–20077. https://doi.org/10.1074/jbc.M111.231878.
Eichwald, C., Arnoldi, F., Laimbacher, A.S., Schraner, E.M., Fraefel, C., Wild, P., Burrone, O.R., Ackermann, M., 2012. Rotavirus Viroplasm Fusion and Perinuclear Localization Are Dynamic Processes Requiring Stabilized Microtubules. PloS One 7, e47947. https://doi.org/10.1371/journal.pone.0047947.
Estes, M.K., Greenberg, H.B., 2013. Rotaviruses. In: Knipe, D.M., Howley, P.M. (Eds.), Fields Virology, sixth ed. Wolters Kluwer Health/Lippincott Williams and Wilkins, Philadelphia, PA, pp. 1347–1401.
Harder, B., Jiang, T., Wu, T., Tao, S., Rojo de la Vega, M., Tian, W., Chapman, E., Zhang, D.D., 2015. Molecular mechanisms of Nrf2 regulation and how these influence chemical modulation for disease intervention. Biochem. Soc. Trans. 43, 680–686. https://doi.org/10.1042/BST20150020.
Holloway, G., Coulson, B.S., 2006. Rotavirus activates JNK and p38 signaling pathways in intestinal cells, leading to AP-1-driven transcriptional responses and enhanced virus replication. J. Virol. 80, 10624–10633. https://doi.org/10.1128/JVI.00390-06.
Irwin, K.K., Renzette, N., Kowalik, T.F., Jensen, J.D., 2016. Antiviral drug resistance as an adaptive process. Virus Evol. 2 vew014. https://doi.org/10.1093/ve/vew014.
Isanaka, S., Guindo, O., Langendorf, C., Matar Seck, A., Plikaytis, B.D., Sayinzoga-Makombe, N., McNeal, M.M., Meyer, N., Adehossi, E., Djibo, A., Jochum, B., Grais, R.F., 2017. Efficacy of a low-cost, heat-stable oral rotavirus vaccine in Niger. N. Engl. J. Med. 376, 1121–1130. https://doi.org/10.1056/NEJMoa1609462.
Jafri, M., Donnelly, B., McNeal, M., Ward, R., Tiao, G., 2007. MAPK signaling contributes to rotaviral-induced cholangiocyte injury and viral replication. Surgery 142, 192–201. https://doi.org/10.1016/j.surg.2007.03.008.
Lecce, J.G., Cummins, J.M., Richards, A.B., 1990. Treatment of rotavirus infection in neonate and weanling pigs using natural human interferon alpha. Mol. Biother. 2, 211–216.
Lee, S.M.-Y., Yen, H.-L., 2012. Targeting the host or the virus: current and novel concepts for antiviral approaches against influenza virus infection. Antivir. Res. 96, 391–404. https://doi.org/10.1016/j.antiviral.2012.09.013.
Li, B., Ding, S., Feng, N., Mooney, N., Ooi, Y.S., Ren, L., Diep, J., Kelly, M.R., Yasukawa, L.L., Patton, J.T., Yamazaki, H., Shirao, T., Jackson, P.K., Greenberg, H.B., 2017. Drebrin restricts rotavirus entry by inhibiting dynamin-mediated endocytosis. Proc. Natl. Acad. Sci. U. S. A 114, E3642–E3651. https://doi.org/10.1073/pnas.1619266114.
Liby, K.T., Sporn, M.B., 2012. Synthetic oleanane triterpenoids: multifunctional drugs with a broad range of applications for prevention and treatment of chronic disease. Pharmacol. Rev. 64, 972–1003. https://doi.org/10.1124/pr.111.004846.
López, S., Oceguera, A., Sandoval-Jaime, C., 2016. Stress response and translation control in rotavirus infection. Viruses 8, 162. https://doi.org/10.3390/v8060162.
McDonald, S.M., Matthijnssens, J., McAllen, J.K., Hine, E., Overton, L., Wang, S., Lemey, P., Zeller, M., Van Ranst, M., Spiro, D.J., Patton, J.T., 2009. Evolutionary dynamics of human rotaviruses: balancing reassortment with preferred genome constellations. PLoS Pathog. 5, e1000634. https://doi.org/10.1371/journal.ppat.1000634.
Moffat, J., Grueneberg, D.A., Yang, X., Kim, S.Y., Kloepfer, A.M., Hinkle, G., Piqani, B., Eisenhaure, T.M., Luo, B., Grenier, J.K., Carpenter, A.E., Foo, S.Y., Stewart, S.A., Stockwell, B.R., Hacohen, N., Hahn, W.C., Lander, E.S., Sabatini, D.M., Root, D.E., 2006. A lentiviral RNAi library for human and mouse genes applied to an arrayed viral high-content screen. Cell 124, 1283–1298. https://doi.org/10.1016/j.cell.2006.01.040.
Mukherjee, A., Patra, U., Bhowmick, R., Chawla-Sarkar, M., 2018. Rotaviral nonstructural protein 4 triggers dynamin-related protein 1-dependent mitochondrial fragmentation during infection. Cell. Microbiol. 20, e12831. https://doi.org/10.1111/cmi.12831.
Niture, S.K., Khatri, R., Jaiswal, A.K., 2014. Regulation of Nrf2—an update. Free Radic. Biol. Med. 66, 36–44. https://doi.org/10.1016/j.freeradbiomed.2013.02.008.
Parashar, U.D., Johnson, H., Steele, A.D., Tate, J.E., 2016. Health impact of rotavirus vaccination in developing countries: progress and way forward. Clin. Infect. Dis. 62, S91–S95. https://doi.org/10.1093/cid/civ1015.
Park, B.K., Boobis, A., Clarke, S., Goldring, C.E.P., Jones, D., Kenna, J.G., Lambert, C., Laverty, H.G., Naisbitt, D.J., Nelson, S., Nicoll-Griffith, D.A., Obach, R.S., Routledge, P., Smith, D.A., Tweedie, D.J., Vermeulen, N., Williams, D.P., Wilson, I.D., Baillie, T.A., 2011. Managing the challenge of chemically reactive metabolites in drug development. Nat. Rev. Drug Discov. 10, 292–306. https://doi.org/10.1038/nrd3408.
Scannevin, R.H., Chollate, S., Jung, M. -y., Shackett, M., Patel, H., Bista, P., Zeng, W., Ryan, S., Yamamoto, M., Lukashev, M., Rhodes, K.J., 2012. Fumarates promote cytoprotection of central nervous system cells against oxidative stress via the nuclear factor (Erythroid-Derived 2)-like 2 pathway. J. Pharmacol. Exp. Therapeut. 341, 274–284. https://doi.org/10.1124/jpet.111.190132.
Shen, Z., He, H., Wu, Y., Li, J., 2013. Cyclosporin a inhibits rotavirus replication and restores interferon-beta signaling pathway in vitro and in vivo. PloS One 8, e71815. https://doi.org/10.1371/journal.pone.0071815.
Silva-Ayala, D., Lopez, T., Gutierrez, M., Perrimon, N., Lopez, S., Arias, C.F., 2013. Genome-wide RNAi screen reveals a role for the ESCRT complex in rotavirus cell entry. Proc. Natl. Acad. Sci. U. S. A. 110, 10270–10275. https://doi.org/10.1073/pnas.1304932110.
Silvestri, L.S., Taraporewala, Z.F., Patton, J.T., 2004. Rotavirus replication: plus-sense templates for double-stranded RNA synthesis are made in viroplasms. J. Virol. 78, 7763–7774. https://doi.org/10.1128/JVI.78.14.7763-7774.2004.
Singh, A., Misra, V., Thimmulappa, R.K., Lee, H., Ames, S., Hoque, M.O., Herman, J.G., Baylin, S.B., Sidransky, D., Gabrielson, E., Brock, M.V., Biswal, S., 2006. Dysfunctional KEAP1-NRF2 interaction in non-small-cell lung cancer. PLoS Med. 3,

e420. https://doi.org/10.1371/journal.pmed.0030420.
Smith, E.M., Estes, M.K., Graham, D.Y., Gerba, C.P., 1979. A plaque assay for the simian rotavirus SA11. J. Gen. Virol. 43, 513–519. https://doi.org/10.1099/0022-1317-43-3-513.
Strasfeld, L., Chou, S., 2010. Antiviral drug resistance: mechanisms and clinical implications. Infect. Dis. Clin. N. Am. 24, 413–437. https://doi.org/10.1016/j.idc.2010.01.001.
Suzuki, M., Otsuki, A., Keleku-Lukwete, N., Yamamoto, M., 2016. Overview of redox regulation by Keap1–Nrf2 system in toxicology and cancer. Curr. Opin. Toxicol. 1, 29–36. https://doi.org/10.1016/J.COTOX.2016.10.001.
Tate, J.E., Burton, A.H., Boschi-Pinto, C., Parashar, U.D., World Health Organization–Coordinated Global Rotavirus Surveillance Network, 2016. Global, regional, and national estimates of rotavirus mortality in children. Clin. Infect. Dis. Off. Publ. Infect. Dis. Soc. Am. 62 (Suppl. 2), S96–S105. https://doi.org/10.1093/cid/civ1013.
To, C., Shilton, B.H., Di Guglielmo, G.M., 2010. Synthetic triterpenoids target the Arp2/3 complex and inhibit branched actin polymerization. J. Biol. Chem. 285, 27944–27957. https://doi.org/10.1074/jbc.M110.103036.
Tong, K.I., Padmanabhan, B., Kobayashi, A., Shang, C., Hirotsu, Y., Yokoyama, S., Yamamoto, M., 2007. Different electrostatic potentials define ETGE and DLG motifs as hinge and latch in oxidative stress response. Mol. Cell. Biol. 27, 7511–7521. https://doi.org/10.1128/MCB.00753-07.
Tong, K.I., Kobayashi, A., Katsuoka, F., Yamamoto, M., 2006. Two-site substrate recognition model for the Keap1-Nrf2 system: a hinge and latch mechanism. Biol. Chem. 387, 1311–1320. https://doi.org/10.1515/BC.2006.164.
Tran, Q.T., Xu, L., Phan, V., Goodwin, S.B., Rahman, M., Jin, V.X., Sutter, C.H., Roebuck, B.D., Kensler, T.W., George, E.O., Sutter, T.R., 2009. Chemical genomics of cancer chemopreventive dithiolethiones. Carcinogenesis 30, 480–486. https://doi.org/10.1093/carcin/bgn292.
Wang, Y.-Y., Yang, Y.-X., Zhe, H., He, Z.-X., Zhou, S.-F., 2014. Bardoxolone methyl (CDDO-Me) as a therapeutic agent: an update on its pharmacokinetic and pharmacodynamic properties. Drug Des. Dev. Ther. 8, 2075–2088. https://doi.org/10.2147/DDDT.S68872.
Weerachayaphorn, J., Luo, Y., Mennone, A., Soroka, C.J., Harry, K., Boyer, J.L., 2014. Deleterious effect of oltipraz on extrahepatic cholestasis in bile duct-ligated mice. J. Hepatol. 60, 160–166. https://doi.org/10.1016/j.jhep.2013.08.015.
Winkel, A.F., Engel, C.K., Margerie, D., Kannt, A., Szillat, H., Glombik, H., Kallus, C., Ruf, S., Güssregen, S., Riedel, J., Herling, A.W., von Knethen, A., Weigert, A., Brüne, B., Schmoll, D., 2015. Characterization of RA839, a noncovalent small molecule binder to Keap1 and selective activator of Nrf2 signaling. J. Biol. Chem. 290, 28446–28455. https://doi.org/10.1074/jbc.M115.678136.
Yin, Y., Chen, S., Hakim, M.S., Wang, W., Xu, L., Dang, W., Qu, C., Verhaar, A.P., Su, J., Fuhler, G.M., Peppelenbosch, M.P., Pan, Q., 2018b. 6-Thioguanine inhibits rotavirus replication through suppression of Rac1 GDP/GTP cycling. Antivir. Res. 156, 92–101. https://doi.org/10.1016/j.antiviral.2018.06.011.
Yin, Y., Dang, W., Zhou, X., Xu, L., Wang, W., Cao, W., Chen, S., Su, J., Cai, X., Xiao, S., Peppelenbosch, M.P., Pan, Q., 2018a. PI3K-Akt-mTOR axis sustains rotavirus infection via the 4E-BP1 mediated autophagy pathway and represents an antiviral target. Virulence 9, 83–98. https://doi.org/10.1080/21505594.2017.1326443.
Zhang, N., Fu, J.N., Chou, T.C., 2016. Synergistic combination of microtubule targeting anticancer fludelone with cytoprotective panaxytriol derived from panax ginseng against MX-1 cells in vitro: experimental design and data analysis using the combination index method. Am. J. Cancer Res. https://doi.org/10.1124/pr.58.3.10.
Zoja, C., Benigni, A., Remuzzi, G., 2014. The Nrf2 pathway in the progression of renal disease. Nephrol. Dial. Transplant. 29, i19–i24. https://doi.org/10.1093/ndt/gft224.